

Enabling In-Bore MRI-Guided Biopsies With Force Feedback

Samuel Frishman¹, Student Member, IEEE, Ali Kight, Student Member, IEEE, Ileana Pirozzi, Student Member, IEEE, Mela C. Coffey², Bruce L. Daniel³, Member, IEEE, and Mark R. Cutkosky⁴, Fellow, IEEE

Abstract—Limited physical access to target organs of patients inside an MRI scanner is a major obstruction to real-time MRI-guided interventions. Traditional teleoperation technologies are incompatible with the MRI environment and although several solutions have been explored, a versatile system that provides high-fidelity haptic feedback and access deep inside the bore remains a challenge. We present a passive and nearly frictionless MRI-compatible hydraulic teleoperator designed for in-bore liver biopsies. We describe the design components, characterize the system transparency, and evaluate the performance with a user study in a laboratory and a clinical setting. The results demonstrate $< 5\%$ difference between input and output forces during realistic manipulation. A user study with participants conducting mock needle biopsy tasks indicates that a remote operator performs equally well when using the device as when holding a biopsy needle directly in hand. Additionally, MRI compatibility tests show no reduction in signal-to-noise ratio in the presence of the device.

Index Terms—Haptic transparency, hydrostatic transmission, MRI-compatible, medical device, needle biopsy, telemanipulation.

I. INTRODUCTION

A. Background and Motivation

MAGNETIC resonance (MR) offers physicians a safe diagnostic and therapeutic imaging modality to detect soft tissue abnormalities (e.g. tumors, inflammation). Innovations in real-time imaging technologies and MR equipment have permitted the application of MR guidance to a growing variety of clinical needs [1]. MRI has potential to provide physicians with live, dynamic views of a target organ during procedures, in addition to preoperative scans. In practice, however, physicians are

Manuscript received September 27, 2019; revised December 29, 2019; accepted January 9, 2020. Date of publication January 15, 2020; date of current version March 17, 2020. This work was supported in part by the NSF and in part by the CHS under Grant 1615891. This article was recommended for publication by Associate Editor C. Duriez and Editor Lynette Jones upon evaluation of the reviewers' comments. (Corresponding author: Samuel Frishman.)

S. Frishman and M. Cutkosky are with the Mechanical Engineering Department at Stanford University, Stanford, CA 94305 USA (e-mail: samuel9@stanford.edu).

A. Kight and I. Pirozzi are with the Bioengineering Department at Stanford University, Stanford, CA 94305 USA (e-mail: akight@stanford.edu; ipirozzi@stanford.edu).

M. Coffey is with the Biomedical Engineering and Mechanics Department, Virginia Tech, Blacksburg, VA 24061 USA (e-mail: mela20@vt.edu).

B. Daniel is with the Radiology Department at Stanford University, Stanford, CA 94305 USA (e-mail: bdaniel@stanford.edu; cutkosky@stanford.edu).

This article has supplementary downloadable material available at <http://ieeexplore.ieee.org>, provided by the authors.

Digital Object Identifier 10.1109/TOH.2020.2967375

1939-1412 © 2020 IEEE. Personal use is permitted, but republication/redistribution requires IEEE permission. See <https://www.ieee.org/publications/rights/index.html> for more information.

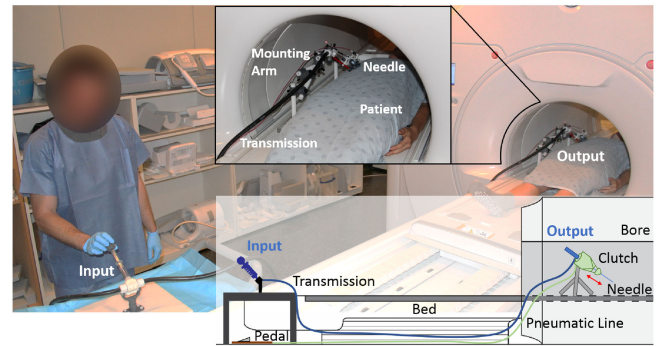


Fig. 1. A hydrostatic teleoperation system transmits forces and motions between a physician standing outside the bore and a biopsy needle within. A pneumatic clutch allows the physician to insert the needle with multiple short strokes, as is common when inserting a needle by hand. Live imaging guides the procedure, eliminating the need to move a patient in and out of the bore.

largely unable to perform percutaneous procedures with live scans due to dimensional constraints imposed by the bore geometry as well as MRI compatibility requirements.

MRI-guided biopsies (e.g. of the liver) are a particularly compelling example of this clinical challenge. Ideally, a physician would have the ability to remotely manipulate a biopsy needle while a patient is being imaged inside the MRI bore. In this vision, interaction forces between the needle and tissue are relayed back to the physician so that they feel as though their fingers are inside the scanner on the needle. This scenario requires equipment to be MRI compatible (i.e. producing negligible imaging artifact or distortion) which severely limits the choices of materials and technologies used for MR-guided interventions.

As an initial application, we focus on MRI-guided liver biopsy. Liver is one of the most common organs to biopsy with the rate of liver cancer increasing in the US [2]. It is projected that liver cancer will be the third largest cancer-related cause of death by 2030 [2]. Moreover, available contrasts (Gadaxetate) allow for clear and prolonged visualization of the liver under MRI [1]. Physicians have access to high contrast images of hepatic tissue for over 30 min with MRI as compared to 30 s with CT. Despite these factors, few MRI-guided solutions exist due to constraints that arise from the limited space between the patient and bore wall.

We present a bidirectional teleoperation system that accurately transmits forces and motions, enabling remote access to a patient's surgical site within the machine (Fig. 1). The

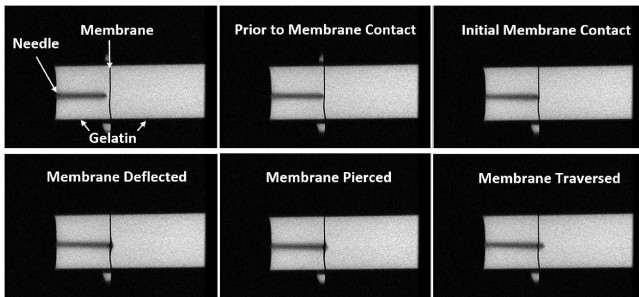


Fig. 2. MRI scans depict the progression of a biopsy needle into a gelatin phantom with an embedded membrane. The images illustrate the limited visual differences between scans at different stages and motivate the need for haptic feedback in MRI guided biopsies.

teleoperator uses a hydrostatic transmission with precision-ground glass pistons and cylinders for high stiffness and nearly frictionless motion. As part of this system we also present an MRI-compatible clutch that can grip and release a biopsy needle. This allows the operator to remotely insert the biopsy needle through multiple strokes in the tight space between the patient and bore wall.

B. Current Standard of Care and Related Work

The current standard of care for biopsies varies depending on the organ and location of suspicious targets. A common method for liver biopsies is described as the stepwise technique where a biopsy needle is iteratively positioned between imaging scans [3]. The patient is pulled in and out of the MRI bore and the needle is inserted a portion of the way each time until the target tissue is reached. This results in prolonged procedural times and preventable errors in needle placement [4]. To improve accuracy, Moche *et al.* [5] explore the use of an external optical system and instrument trackers that provide updated needle visualization overlaid on an initial scan. For other organs such as the prostate, a similar paradigm is often used. Specifically, in MRI-TRUS fusion biopsy, an initial MRI scan is fused with live ultrasound [6]. These methods seek to benefit from the superior imaging quality of MRI while providing live visualization.

Other groups have developed devices with MRI-compatible actuators [7]. Examples include piezoelectric motors [8], [9], pneumatic motors [10], electroactive polymers [11] and hydraulics [12]. The location of the prostate allows these devices to be placed near the patient along the axis of the bore where there is substantial space. However, to access the liver (as well as other organs such as the breast) the device must be significantly more compact to fit between the patient and bore wall. In one approach, for both MRI and CT, groups place a significant portion of the actuation system outside the scanner and utilize a robotic arm to reach inside the bore [13], [14].

Most robotic devices do not provide haptic feedback, and their precision is limited by image quality. Haptic feedback is particularly important in needle insertion tasks where vision is limited [15]. Despite its advantages over other diagnostic imaging modalities, MRI is subject to slow acquisition rates and relatively low-resolution images as compared, for

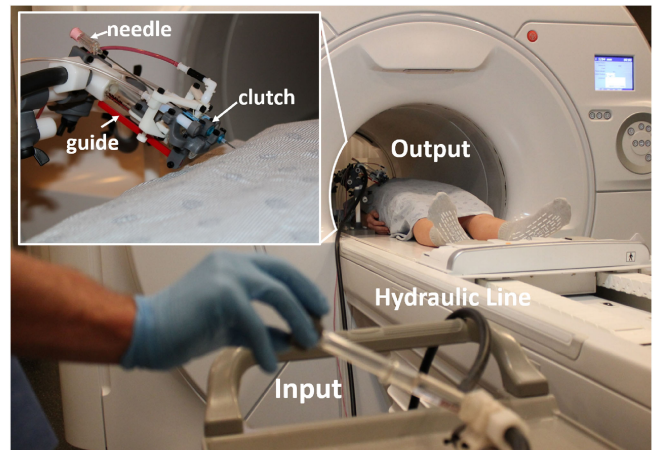


Fig. 3. A physician pushes an input cylinder and uses a foot pedal to actuate a pneumatic clutch (inset) to grasp and release the needle. Incremental insertion enables the device to fit alongside the patient inside the MRI bore.

example, to cameras used in endoscopy. Furthermore, biopsy needles often cause imaging artifacts. As a result, exact needle tip position is often unknown from imaging alone. Even in a simplified scenario, such as that illustrated in Fig. 2, where a silicone membrane produces a clear black line in the MRI image, the difference between membrane *contact* and *puncture* is difficult to discern. Nevertheless, precise needle placement is of growing importance. In particular, as the interest in tumor microenvironments and heterogeneity grows [16], the need for procedural precision in biopsies becomes critical. Physicians want not only a sample of the tumor itself but also of surrounding tissue to understand tumor evolution and inform treatment decisions.

Franco *et al.* [17] address the challenge of liver biopsy with a pneumatically actuated device for needle alignment inside the MRI bore. However, they indicate that insertion itself is performed manually outside the bore, despite the reduction in accuracy, because of difficulties associated with inserting the needle in such a confined environment, as well as safety and cost benefits resulting from manual insertion. Our proposed clutching device enables insertion of a long, stiff needle through multiple short strokes and, as a passive system, maintains the safety of manual insertion.

II. DESIGN

MRI compatibility requirements limit the choice of materials and technologies used for MRI-guided interventions. Ferrous components of any kind are incompatible, and even non-ferrous materials can cause image distortions. As noted above, the MRI bore's dimensions constrain the size and motion range available for an interventional device. To address these issues we have developed an MRI-compatible teleoperator that includes a multi-axis mounting arm for setting the initial needle alignment (Fig. 1). The device uses a hydrostatic transmission to enable access inside the MRI bore and a clutching mechanism to incrementally insert a biopsy needle (Fig. 3).

Hydraulic transmissions are a compelling choice for teleoperation as they can be designed to be MRI-compatible and

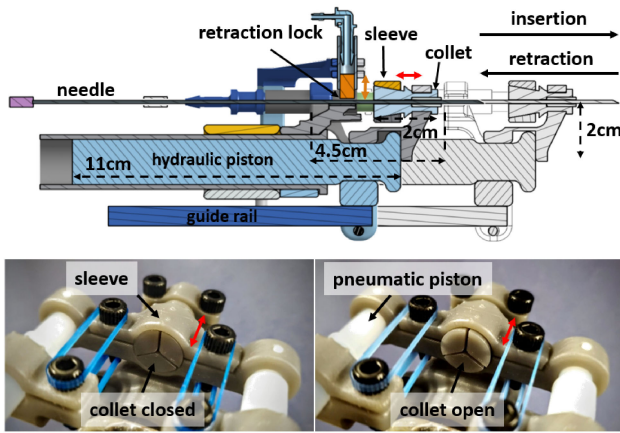


Fig. 4. (Top) Cross-section of the clutch design. A pneumatically actuated sleeve compresses the collet around the needle. A second piston locks the needle position when the collet releases. After an input stroke, the clutch is released and the hydraulic piston is retracted to re-grip the needle at a higher position. In its initial configuration, the device is shorter than the needle, enabling it to fit inside the bore. (Bottom) A demonstration of the collet opening to release the needle when an operator steps on the foot-pedal.

have the ability to route in compact spaces. In standard 60-70 cm diameter scanners there is only a ≈ 20 cm gap between the patient's skin and the inner wall of the bore (assuming an average body mass index). Biopsy needles are up to 15 cm long and consume a significant portion of this gap, leaving little room for a device. To address the space constraints and still reach the necessary insertion depths, a key component of our design is a custom MRI-compatible needle clutch that grips and releases the needle (Fig. 4). Using the clutch, the needle is inserted through multiple short strokes. This is similar to how a physician would drive a needle if holding it directly in hand; gripping it close to the tip, inserting part way, re-gripping further up, and inserting deeper. The transmission and clutch are described below.

A. Transmission

Haptic transparency of a transmission (how well forces and vibrations propagate between the input and output) depends on its stiffness and friction. With suitable tubing, hydraulic systems are inherently stiff. However, traditional hydraulic seals introduce stick-slip friction, which is undesirable for haptic applications. Users tolerate and adapt to modest amounts of added inertia, viscous friction, and hysteresis; however, the severe nonlinearities of stick-slip friction and backlash are harder to accommodate [18].

At each end of the transmission we use custom pistons and cylinders adapted from ground glass syringes employed in the Loss of Resistance technique for locating the epidural space in the spine [19]. We modify B. Braun 10 ml glass syringes¹ by dry polishing the plunger (piston) and barrel (cylinder) and cutting away the end of the barrel to eliminate any reduction in diameter. Pipe constrictions are undesirable given that resulting friction losses grow with the ratio of diameters to the

fourth power for $Re < 2500$ [20]. We selected 10 ml syringes as they offer sufficient insertion depth (up to 5 cm) per clutch stroke and maintain a small form factor. Larger and smaller pistons can be designed for other applications.

If used with saline, as in epidural procedures, the pistons are prone to occasional binding against the cylinders. Instead, a silicone oil² was selected as the working fluid. The 5 cSt oil is human-safe and represents the lowest viscosity we have found that does not evaporate at room temperature and pressure.

The gap between the piston and cylinder is 0.015 mm. This results in a seal with little leakage. For large ratios of diameter-to-gap, the piston and bore can be modeled as flat plates and leakage is computed as laminar flow between two parallel plates [21]. At maximum operating forces expected during a biopsy procedure (20 N) leakage is ≈ 0.02 ml/min. If used clinically, the output cylinder can be covered with a bellows or flexible bag, as employed for other medical devices for sanitation [22].

The transmission uses reinforced tubing ($d_{tube} = 9.5$ mm inner diameter, McMaster #5645K25). The tubing was sized to be similar to the piston diameter ($d_{cyl} = 15$ mm) to reduce flow restrictions while maintaining a minimum bend radius of $r \approx 10$ cm. Larger tubing will reduce viscous losses but increase inertia and minimum bend radius. Reinforced tubing improves transparency by reducing the compliance associated with tube expansion under pressure. The input displacement (with the output fixed) resulting from tubing compliance can be approximated by $\delta = ((2\sqrt{L}f_{in}d_{tube}^2)/(\pi t_{tube}Ed_{cyl}^3))^2$ [21]. For a tubing length of $L = 3.5$ m and an input force of $f_{in} = 20$ N (with E and t_{tube} corresponding to the Young's modulus and wall thickness of the tubing described above), we estimate a maximum deflection of $\delta < 0.015$ mm resulting from tubing expansion.

Two systems were constructed, one for use in the MRI facilities and a shorter version for laboratory experiments (3.5 m and 1.5 m respectively). The 3.5 m version enables the input to be located at the end of the MRI scanner's bed while the output is inside the MRI bore at the imaging center (Fig. 3). This arrangement keeps the input outside the 5 Gauss limit where it is safe to have electrical components, such as computer monitors to display MRI scans.

B. Clutch

Insertion of a biopsy needle in a single stroke is impractical [17]. Accordingly, we created a pneumatically actuated clutch that grips and releases the needle (Figs. 3, 4) to insert with multiple strokes.

The clutch utilizes a collet mechanism (Fig. 4) of 3D-printed plastic (Engineering Resins Grey Pro and Tough). The collet is segmented into three leaflets with internal grooves on the surfaces that contact the needle to provide an exit path for fluid. The collet is 2 cm long, consuming less than 15% of a 15 cm biopsy needle. The collet provides a maximum axial grip force of 25 N, well above the expected forces for a liver

¹ <https://www.bbraunusa.com/en/products/b/loss-of-resistancesyringes.html>

² <http://www.clearcoproducts.com/pure-silicone-low-viscosity.html>

biopsy. It is possible to adjust the maximum gripping force by changing the number of elastic bands (visible in Fig. 4).

In the closed state, elastic bands slide a sleeve over the collet, forcing the leaflets to close around the needle and form a tight grip (Fig. 4). To open the collet, the operator steps on a foot pedal that actuates pneumatic pistons to slide the sleeve off the collet, which expands elastically, releasing the needle. Once the needle is released, the operator can retract and re-grip the needle higher up. When the collet is open, a retraction lock is activated, ensuring that the needle remains fixed during retraction of the piston.

III. EVALUATION

Force and motion requirements for MRI guided biopsy procedures are described in [17], [23]. In summary, liver biopsy insertion depths range from 5-11 cm with a mean target size of 1.5-3 cm diameter [5]. The maximum expected force on the needle is ≈ 20 N, and dynamic force variations of 0.5-1.5 N are of interest as they indicate events such as a puncture [24].

Experiments were performed to assess device performance. We evaluated the system transparency and conducted user tests in realistic tissue phantoms in lab and clinical settings (i.e. inside the MRI room).

A. System Transparency

A system identification was performed to determine the system's ability to track forces between the input and output. Force sensors (Futek FSH00103 and Omega LCFD-5, resolution ≈ 10.6 mN) were mounted at each end, and the input was oscillated by a muscle lever (Cambridge Tech., Model 6900) with the output fixed against a hard stop. An up-chirp signal swept input frequencies from 0.2-200 Hz. Data were recorded on an Arduino Due at 500 Hz.

B. User Tests

A user study (IRB-26526) was conducted to determine an operator's ability to detect important cues that occur during biopsy procedures, such as input force spikes as the needle punctures an organ or tumor, and to evaluate the role of haptics in identifying these events. The study included 10 participants: 5 men, 5 women, ages 24-29, 1 left handed. All participants had some experience with haptics research and teleoperation but were novices in needle insertion tasks. Participants inserted an 18 gauge, bevel-tip biopsy needle into phantom tissue with an embedded membrane mimicking a liver (fabrication details in the following section). Users were instructed to stop insertion when they detected the membrane. The amount of membrane deflection was recorded via an overhead camera. Users were then instructed to continue insertion until they determined that the needle had punctured the membrane. The amount of overshoot beyond the membrane was recorded, again via overhead camera. Three cases were evaluated: (i) the user inserts the needle directly by hand with the phantom in view (the phantom is semi-transparent, so the user can see the needle inside the mock tissue); (ii) the user inserts

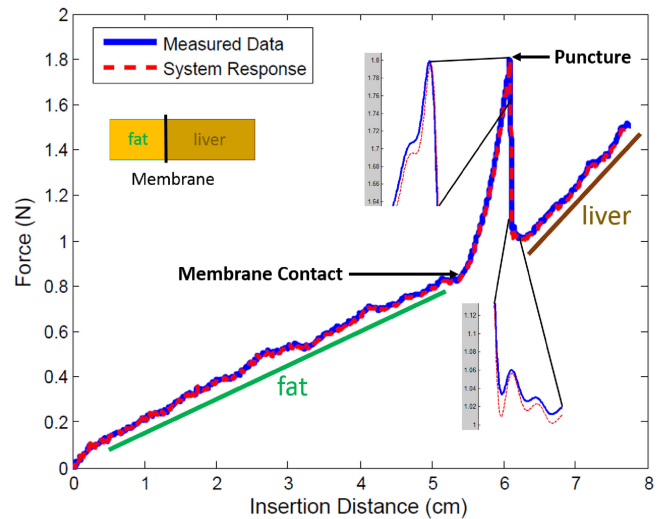


Fig. 5. Example force profile inserting an 18 G biopsy needle into the phantom. Two force slopes are visible and mimic the properties of fat and liver tissue. The puncture force is sized to match liver punctures. The system response to the insertion force profile is also shown. The response is computed using the transfer function from frequency analysis (Fig. 6).

the needle directly by hand with the phantom occluded (the user is forced to rely on haptic feedback alone); (iii) the user inserts the needle using the teleoperator (the phantom is again not visible so the user must rely on haptic feedback). Four phantom configurations were used which included combinations of two surface-to-membrane depths (5.5 cm and 8 cm) and two levels of membrane hardness (30 and 10 Shore A) which translate to puncture forces of ≈ 1.5 N and ≈ 0.75 N, respectively. Insertion depths and forces were selected to be in the range of those occurring during liver biopsy procedures. When using the teleoperator, phantoms were presented to the user in pseudo-random order and each phantom was presented to the user three times. In the cases where the user held the needle directly in hand, each phantom was punctured four times (two per case). In total, each user conducted 28 insertions. Users completed a SURG-TLX post-questionnaire after the study [25].

Membrane deflection and needle overshoot were determined using the ratio of pixel distances and a known length (markings on the needle) in the image. This method was tested on known distances and was accurate to 0.1 mm.

1) *Phantom Design*: Phantoms were created to replicate human tissue material properties and mimic the forces experienced in liver biopsy procedures. The phantom is comprised of two halves separated by a membrane (Fig. 5), with the halves representing the properties of fat and liver tissue. Appropriate force profiles for inserting a biopsy needle in true fatty tissue and into a liver are documented [24], [26]. Weight ratios of 1:8 and 1:7 gelatin (Knox unflavored) to water were used to replicate the tissue types and were found to match the force slopes for fat and liver tissue found in [26].

When transitioning between tissue types, there is a force spike at the needle. To simulate this interface, the phantom contained an embedded membrane between the two sections

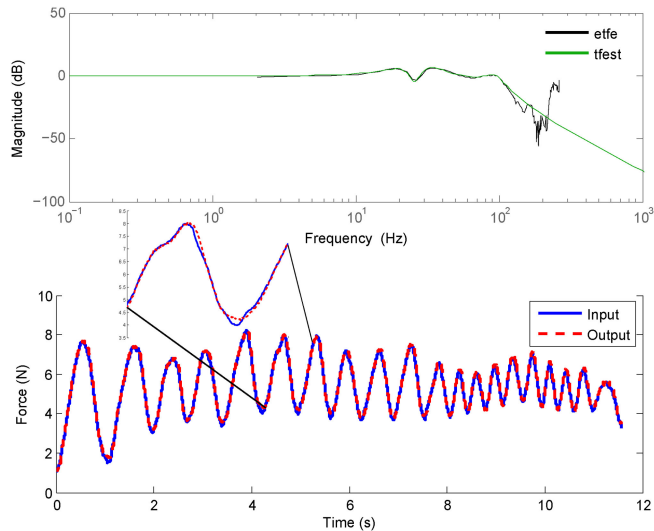


Fig. 6. Top: Force magnitude frequency analysis (etfe and tfest in MATLAB). Force sensors were placed at either end of the system and the input was oscillated using an up-chirp signal (0.2-200 Hz). Bottom: Force tracking with the input manipulated by hand and the output fixed against a spring. Magnified inset shows that small force errors occur mainly during motion reversals.

of gelatin. The membrane was made of a 0.8 mm thick silicone layer (Smooth-On Dragon Skin 30 and 10), chosen to match the range of puncture forces expected when inserting a biopsy needle into a liver [24]. Furthermore, the silicone hardness was selected to be in the range of common tissues biopsied, including the liver [27]. Membranes were embedded in the gelatin at two depths (5.5 cm and 8 cm), resulting in four combinations of phantom tissue depth and hardness. The phantom's cross section formed a 5x5 cm square and insertions were limited to the central 2.5x2.5 cm region to minimize edge effects at the periphery of the membrane.

C. Clinical Use

1) *MRI Compatibility*: The system is constructed entirely of non-conductive materials (plastics, ceramics, rubbers); nevertheless, an MRI compatibility test was performed to ensure it had negligible impact on the imaging quality. A GE phantom was scanned with and without the device (using SSFSE and 3D LAVA sequences) and the signal-to-noise ratio (SNR) between the cases was compared.

2) *Experiments With Real-Time MRI Scans*: To validate the system performance in a clinical setting, a phantom biopsy task was performed by an interventional radiologist at the Stanford Lucas Center for Imaging. As in the previously described user study, the radiologist was instructed to insert the biopsy needle into a phantom until the membrane was detected and then puncture the membrane with minimum overshoot. In addition to the haptic feedback received through the transmission, the radiologist could view MRI scans on a computer screen during insertion to visualize the location of the needle. A SSFSE single slice sequence (4 s acquisition time) was selected to provide a relatively fast image update whenever a scan was requested. Though faster sequences are possible with frame rates near 1 Hz, image

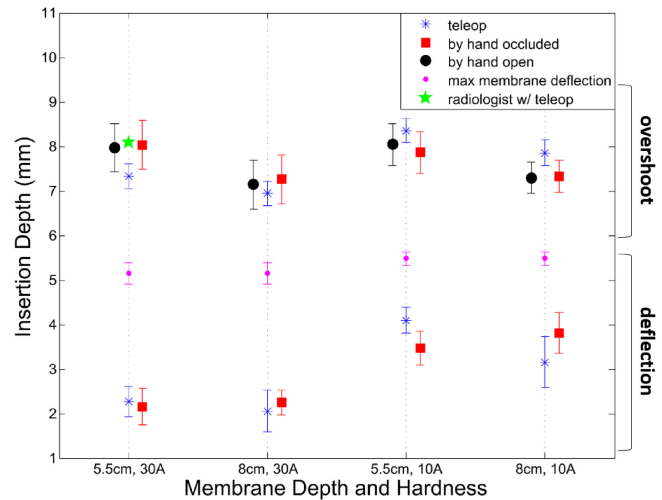


Fig. 7. Average membrane deflection and depth beyond puncture (overshoot) across ten participants for the four phantom configurations. The maximum deflection a membrane can withstand prior to puncture is also shown; overshoot is the distance past this maximum deflection. Puncture depth from a single trial with an interventional radiologist and live MRI scans is presented as a single point in green.

quality is reduced and precise slice alignment with the needle is required. In practice, it is common for some scan sequences to take 3-5 min.

IV. RESULTS

A. System Transparency

System identification indicates a 75 dB roll-off at ≈ 100 Hz (Fig. 6). The system also exhibits two resonant modes (at 20 Hz and 35 Hz) corresponding to the input and output mounting structures. Near unity tracking is observed during typical manipulation speeds (< 20 mm/s) and interaction forces ($0 \leq f \leq 8$ N) (Fig. 6 bottom). In the example shown, average RMS force error ($\sqrt{(f_{in} - f_{out})^2 / f_{in}}$) is $\approx 4\%$ with the majority of error occurring during direction changes.

With no resistance at the output, input force at a constant speed of 10 mm/s is ≈ 0.05 N. This is primarily a result of viscous losses and increases linearly with speed [28]. At typical needle insertion speeds, the viscous losses can be considered negligible compared to the friction force experienced by the needle inside tissue.

B. User Study

Figure 7 shows the average membrane deflection and overshoot for the four phantom configurations. No statistically significant difference in overshoot is observed between the three insertion cases. However, overshoot is reduced in the two phantom configurations where the membrane is embedded deeper in the mock tissue.

Membrane deflection is only compared between the occluded and teleoperation cases (case 2 and 3). When vision is present (case 1), a user can see the needle and contact the membrane with negligible deflection. Little difference is observed between holding the needle in hand (case 2) vs. using

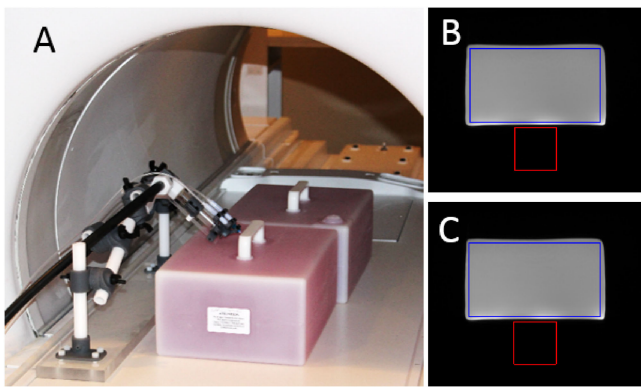


Fig. 8. (A) Device positioned with two GE phantoms. LAVA scan of the phantom without (B) and with (C) the device. Regions of interest used to calculate SNR are shown with blue and red boxes. Difference in SNR values is negligible.

the teleoperator (case 3); however, deflection is increased for the two phantom configurations with softer membranes.

When inserting the needle by hand with the phantom occluded, a total of four false positive detections and one missed detection occurred across the ten users (a false positive occurs when a user indicates they feel the membrane before the needle makes contact). Combined, this amounts to 6.25% of insertions performed under this condition. With the teleoperator, five false positives occurred and three missed detections (a combined 6.67%). In the false positive cases, users corrected their mistake when instructed to continue inserting the needle. In cases where detection of membrane contact was missed, users still perceived membrane puncture.

C. MRI Compatibility

The MRI compatibility tests found negligible change in imaging SNR with placement of the device near the phantom (0.55% and 0.17% for the 3D LAVA sequence and SSFSE sequence respectively). These values are much smaller than those reported for some other robotic systems intended for MRI [8]. The device configuration, sample scans, and regions-of-interest are shown in Fig. 8.

D. Experiments With Real-Time MRI Scans

The interventional radiologist was able to detect and pierce the membrane using the teleoperation device. Membrane overshoot is plotted in Fig. 7 as a single point and is close in value to users conducting the similar task in a lab setting. The radiologist utilized four SSFSE single slice scans. These included an initial scan to visualize the needle and phantom, a second scan to visualize the needle approaching the membrane, a third scan when membrane contact was perceived, and a fourth scan to confirm puncture.

V. DISCUSSION

The transmission provides haptic transparency with sufficient bandwidth to enable force transients and vibrations to propagate through the system. This is important for perception of

tissue texture and dynamic forces given that human mechanoreception is responsive to frequencies in range of hundreds of Hz [29]. Additionally, viscous losses resulting from the transmission are small compared to frictional forces experienced in a biopsy procedure and have little impact on the operator's ability to sense changes in input force. The system can be improved further with stiffer hydraulic tubing (e.g. aramid braided hose) and increased rigidity of the input and output structures.

The user tests indicate that there is no statistically significant difference in membrane overshoot between the three insertion cases. Surprisingly, the case with vision (case 1) had the same level of membrane overshoot as the other two cases. This suggests that overshoot was largely a result of inherent dynamics in a human arm/hand which are dominant compared to the teleoperator. As a result, regardless of whether the user can see the membrane (which would be unrealistic in the application scenario) and whether the user is holding the needle in hand or using the teleoperator, they are limited to how quickly they can stop insertion when the puncture is perceived. These critical moments may be missed with MRI alone due to relatively slow frame rates and imaging quality, emphasizing the importance of haptic feedback in MRI-guided tasks. The overshoot is also reduced in the cases where the membrane is embedded deeper in the phantom. This is likely due to increased friction, which stops motion faster, and suggests that increasing damping in the teleoperator (e.g. by using a higher viscosity oil) may improve accuracy. On the other hand, increasing viscosity has some undesirable consequences and further experimentation is necessary to determine system parameters that balance the effects.

Although haptic feedback alone is adequate in these experiments, vision is still necessary in true biopsy procedures as the environment is more complex than a single membrane. The needle may be traversing several tissue types and have multiple degrees of freedom. Furthermore, the presence of vision did reduce mental demand, task complexity, and situational stress for users based on the SURG-TLX post-questionnaire. Of course, in true biopsy procedures, the physician cannot see into the patient and must use imaging modalities to view the needle. In the test case with live MRI scans and an interventional radiologist, the radiologist used scans to position the needle near the membrane and subsequently relied on haptic feedback to perform the puncture. This suggests a paradigm where MRI scans and haptic feedback provide complementary functions: scans provide approximate positioning of the needle and haptic feedback is used for precise insertion and event detection. This strategy has the potential to reduce biopsy duration by decreasing the number of scans necessary and improve accuracy by leveraging combined sensory modalities.

Participants had an intuitive understanding of incremental needle insertion via the clutching mechanism and had little difficulty adapting to the technique. We recorded some trials during which users actuated the clutch when the needle was positioned immediately before or on the membrane. In these instances, users were still able to detect the membrane; however, they reported less confidence. This may be because the puncture force was not preceded by a gradual increase, as

when a needle moves steadily through the phantom without interruption. In these instances, participants used perceived force magnitude and the elasticity of the mock tissue to determine membrane contact. Several users indicated that membrane elasticity played an important role: they could feel the increased stiffness of the membrane as compared to gelatin.

Additional interesting cases arose when substantial needle bending occurred. The needle is bevel-tipped and prone to bend during insertion, which increases the insertion force. This effect in part motivates enabling live imaging during a procedure. In our tests, users were still able to detect the membrane in the majority of instances when needle bending was evident. This again suggests that they utilized not only the force magnitude but also changes in stiffness.

Both by hand and with the teleoperator, several false positives and missed detections occurred. Insertion speed, needle deflection, and user experience may play a role in these cases (four users detected all membranes correctly). Though undesirable, these false positives and missed detections, in particular those that occur when holding the needle directly in hand, demonstrate the difficulty of the task and the realistic nature of the phantom design.

VI. CONCLUSION

We have presented a teleoperator that enables in-bore MRI-guided biopsies with haptic transparency. The teleoperator includes a stiff, low-friction hydrostatic transmission and a pneumatic clutching mechanism for incremental needle insertion.

System characterization and experiments with users demonstrate the system performance. Near unity force tracking is observed at realistic manipulation speeds. Operators using the device can insert a biopsy needle with the same accuracy as if holding the needle directly in hand. The system is constructed of non-conductive materials and has negligible impact on imaging SNR. The inherent safety and low cost of a passive system can facilitate its adoption, as a step towards clinical use of in-bore MRI guided interventions.

The next step is to extend teleoperation to multiple axes such that a physician can adjust needle orientation during insertion. High fidelity haptic feedback is less critical in these positioning degrees of freedom and actuation can be achieved with more traditional hydraulic actuators or other mechanisms. Low friction and backdrivability remain important, however, as they will enable the system to adapt passively to a patient's physiological motions.

ACKNOWLEDGMENT

This work is supported in part by NSF CHS 1615891. The authors would like to thank Vipul Sheth, Gary Glover, Kevin Epperson, and Karla Epperson for their help at the Stanford Lucas Center of Imaging. They would also like to thank Brent Gillespie (U. Mich.) for his suggestion to consider loss of resistance syringes.

REFERENCES

- [1] J. Weiss, R. Hoffmann, and S. Clasen, "MR-guided liver interventions," *Topics Magn. Reson. Imag.*, vol. 27, no. 3, pp. 163–170, 2018.
- [2] L. Rahib, B. D. Smith, R. Aizenberg, A. B. Rosenzweig, J. M. Fleshman, and L. M. Matrisian, "Projecting cancer incidence and deaths to 2030: The unexpected burden of thyroid, liver, and pancreas cancers in the united states," *Cancer Res.*, vol. 74, no. 11, pp. 2913–2921, 2014.
- [3] J. Tokuda *et al.*, "In-bore setup and software for 3t mri-guided transperineal prostate biopsy," *Phys. Medicine Biol.*, vol. 57, no. 18, 2012, Art. no. 5823.
- [4] N. V. Tsekos, A. Khanicheh, E. Christoforou, and C. Mavroidis, "Magnetic resonance-compatible robotic and mechatronics systems for image-guided interventions and rehabilitation: A review study," *Annu. Rev. Biomed. Eng.*, vol. 9, pp. 351–387, 2007.
- [5] M. Moche *et al.*, "Navigated mri-guided liver biopsies in a closed-bore scanner: experience in 52 patients," *Eur. Radiol.*, vol. 26, no. 8, pp. 2462–2470, 2016.
- [6] M. M. Siddiqui *et al.*, "Magnetic resonance imaging/ultrasound-fusion biopsy significantly upgrades prostate cancer versus systematic 12-core transrectal ultrasound biopsy," *Eur. Urology*, vol. 64, no. 5, pp. 713–719, 2013.
- [7] H. Elhawary, Z. T. H. Tse, A. Hamed, M. Rea, B. L. Davies, and M. U. Lamberth, "The case for mr-compatible robotics: A review of the state of the art," *Int. J. Med. Robot. Comput. Assisted Surgery*, vol. 4, no. 2, pp. 105–113, 2008.
- [8] P. Moreira *et al.*, "The miriam robot: A novel robotic system for mr-guided needle insertion in the prostate," *J. Med. Robot. Res.*, vol. 2, no. 04, 2017, Art. no. 1750006.
- [9] H. Su *et al.*, "Piezoelectrically actuated robotic system for mri-guided prostate percutaneous therapy," *IEEE/ASME Trans. Mech.*, vol. 20, no. 4, pp. 1920–1932, Aug. 2015.
- [10] M. Muntener *et al.*, "Transperineal prostate intervention: Robot for fully automated mr imaging system description and proof of principle in a canine model," *Radiology*, vol. 247, no. 2, pp. 543–549, 2008.
- [11] K. Tadakuma, L. M. DeVita, J.-S. Plante, Y. Shaoze, and S. Dubowsky, "The experimental study of a precision parallel manipulator with binary actuation: With application to mri cancer treatment," in *Proc. IEEE Int. Conf. Robot. Autom.*, 2008, pp. 2503–2508.
- [12] M. R. Van den Bosch *et al.*, "Mri-guided robotic system for transperineal prostate interventions: proof of principle," *Phys. Medicine Biol.*, vol. 55, no. 5, 2010, Art. no. N133.
- [13] A. Melzer *et al.*, "Innomotion for percutaneous image-guided interventions," *IEEE Eng. Medicine Biol. Mag.*, vol. 27, no. 3, pp. 66–73, May-Jun. 2008.
- [14] D. A. Schreiber, D. B. Shak, A. M. Norbash, and M. C. Yip, "An open-source 7-axis, robotic platform to enable dexterous procedures within ct scanners," 2019, *arXiv:1903.04646*.
- [15] O. Gerovich, P. Marayong, and A. M. Okamura, "The effect of visual and haptic feedback on computer-assisted needle insertion," *Comput. Aided Surgery*, vol. 9, no. 6, pp. 243–249, 2004.
- [16] M. R. Junttila and F. J. de Sauvage, "Influence of tumour micro-environment heterogeneity on therapeutic response," *Nature*, vol. 501, no. 7467, 2013, Art. no. 346.
- [17] E. Franco, D. Bruijic, M. Rea, W. M. Gedroyc, and M. Ristic, "Needle-guiding robot for laser ablation of liver tumors under mri guidance," *IEEE/ASME Trans. Mechatronics*, vol. 21, no. 2, pp. 931–944, Apr. 2016.
- [18] V. Hayward and K. E. MacLean, "Do it yourself haptics: Part I," *IEEE Robot. Autom. Mag.*, vol. 14, no. 4, pp. 88–104, Dec. 2007.
- [19] B. D. Butler, R. D. Wartars, J. R. Elk, I. Davies, and E. Abouleish, "Loss of resistance technique for locating the epidural space: Evaluation of glass and plastic syringes," *Can. J. Anaesthesia*, vol. 37, no. 4, pp. 438–439, 1990.
- [20] C. C. E. Division, *Flow of Fluids Through Valves, Fittings, and Pipe*. Stamford, CT, USA: Crane Company, 1957, Art. no. 410.
- [21] S. P. Buerger, "Stable, high-force, low-impedance robotic actuators for human-interactive machines," PhD dissertation, Dept. Mech. Eng., Mass. Inst. of Tech., Cambridge, MA, USA, 2005.
- [22] M. J. Latif and B. J. Park, "Robotics in general thoracic surgery procedures," *J. Visualized Surgery*, vol. 3, no. 4, pp. 44–53, 2017.
- [23] N. Burkhard *et al.*, "A rolling-diaphragm hydrostatic transmission for remote mr-guided needle insertion," in *Proc. IEEE Int. Conf. Robot. Autom.*, 2017, pp. 1148–1153.
- [24] J. D. Westwood *et al.*, "In vivo force during arterial interventional radiology needle puncture procedures," in *Medicine Meets Virtual Reality: The Magical Next Becomes the Medical Now*, Amsterdam, The Netherlands: IOS Press, 2005, vol. 111, pp. 178–184.
- [25] M. R. Wilson, J. M. Poolton, N. Malhotra, K. Ngo, E. Bright, and R. S. Masters, "Development and validation of a surgical workload measure: The surgery task load index (surg-tlx)," *World J. Surgery*, vol. 35, no. 9, 2011, Art. no. 1961.

- [26] S. Jiang, P. Li, Y. Yu, J. Liu, and Z. Yang, "Experimental study of needle-tissue interaction forces: Effect of needle geometries, insertion methods and tissue characteristics," *J. Biomechanics*, vol. 47, no. 13, pp. 3344–3353, 2014.
- [27] Y. C. Yoon, J. S. Lee, S. U. Park, J. H. Kwon, T. H. Hong, and D. G. Kim, "Quantitative assessment of liver fibrosis using shore durometer," *Ann. Surgical Treatment Res.*, vol. 93, no. 6, pp. 300–304, 2017.
- [28] A. Gruebele, S. Frishman, and M. R. Cutkosky, "Long-stroke rolling diaphragm actuators for haptic display of forces in teleoperation," *IEEE Robot. Autom. Lett.*, vol. 4, no. 2, pp. 1478–1484, Apr. 2019.
- [29] D. A. Mahns, N. Perkins, V. Sahai, L. Robinson, and M. Rowe, "Vibrotactile frequency discrimination in human hairy skin," *J. Neurophysiology*, vol. 95, no. 3, pp. 1442–1450, 2006.